Examination of the Relationship Between Tuned Free Vibration Characteristics and Mistuning Sensitivity for an Industrial Turbomachinery Rotor

Mahmoud I. Hussein
Graduate Student

Matthew P. Castanier
Assistant Research Scientist

Christophe Pierre
Professor

Report No. UM-ME-01-06

December 2000
Revised October 2001

Department of Mechanical Engineering
The University of Michigan
Ann Arbor, Michigan 48109-2125
U.S.A.

Abstract

The inevitable occurrence of blade mistuning in turbomachinery rotors drastically increases the possibilities of vibration localization. This in turn increases the likelihood of an excessive vibration response at certain conditions, thus posing a major safety concern. The characteristics of tuned system free vibrations, in relation to the operation conditions, are shown to have direct correlations with the degree of mistuning sensitivity. In this work, mistuned forced response data from a reduced order model (ROM) is used to establish such relationships. Furthermore, the underlying physical mechanisms are explored, and general guidelines are presented as an inexpensive design tool for early assessments of mistuning sensitivity.

1. Introduction

In practice, the individual sectors that comprise a turbomachinery rotor are seldom identical. There are always small variations in the structural properties of individual blades, which may be attributed to manufacturing and material tolerances or in-service degradation. These blade-to-blade variations are commonly referred to as blade mistuning. Since a bladed disk is a periodic structure (Figure 1a), these small irregularities may inhibit the even distribution of vibration energy among the blades, and result in vibration localization. This phenomenon is a major source of safety concern because in some cases vibration energy may be confined to only a few blades, thus resulting in excessive deflections. Normal mode localization has attracted considerable interest in solid state physics [1-4], and later in the structural dynamics field [5-12].

The simplest approach to predict the extent of localization, and its effect on the overall response, is to solve for the forced response of the entire mistuned system for every possible irregular configuration. Such route entails enormous computational effort for obvious reasons. Recently Bladh *et al.* [13] developed an accurate and efficient ROM technique, utilizing cyclic symmetry, component mode synthesis and statistical methods to predict the mistuned forced response. This technique promises to be a highly effective tool for accurately predicting mistuning sensitivity (MS), which is defined here as the ratio of the maximum mistuned forced response amplitude to that of the equivalent tuned system.

On another track, there are ongoing efforts to establish a way of predicting mistuning sensitivity solely from information describing the tuned free vibration characteristics and the operation conditions. If such connection, and the associated relationships, can be thoroughly understood, an inexpensive design tool for early assessments of mistuning sensitivity can be provided. The aim of this study is to examine these relationships.

The tuned free vibration characteristics can be derived from an eigenfrequency versus number of nodal diameters plot, such as the one displayed in Figure 2. The number of nodal diameters refers to the lines of zero displacement across the diameter of the disk. One of the significant features of this plot is the curve veerings of eigenfrequency loci. Previous work [10] has shown that this free vibration characteristic, in any disordered periodic system, has implications on mode localization. In fact, it was shown that mode localization and eigenfrequency loci veering are two manifestations of the same phenomenon. This implies that mistuning sensitivity is expected to increase at operating points close to veerings in the eigenfrequency plot. In the context of bladed disk analyses, Bladh *et al.* [14] recently devised a method to calculate eigenfrequencies for interblade phase angles that are between those corresponding to integer numbers of nodal diameters. This, in essence, provides a tool for obtaining continuous plots of the eigenfrequency versus the number of nodal diameters, hence an opportunity to better capture veerings. With this tool in hand it becomes possible to investigate the relationship between the characteristics of curve veerings and mistuning sensitivity. It also becomes feasible to examine the significance of how close a veering is to the point of operation.

The relationship between the free vibration characteristics and mistuning sensitivity can also be described physically. For example, it is well known [12] that for a mistuned bladed disk the degree of structural interblade coupling has a direct effect on mode localization. The structural coupling is governed by the stiffness properties of the disk-blade sector and its connectivity to adjacent sectors. In a structural model of an unshrouded bladed disk, it is conceivable that the only means of energy transmission from one blade to the next is through the disk. It is therefore reasonable to assume that the structural interblade coupling is related to the amount of interaction between disk- and blade-dominated modes. On this basis, one can assume that the variation of the degree of coupling from one state of operation to another depends on the ratio of disk to blade participation. A direct indication of the relative level of disk participation is the slope of the eigenfrequency loci at the point of operation. The relative level of disk participation can also be related to the characteristics of curve veerings. Hence, by

correlating eigenfrequency characteristics with forced response data, a connection can be established between physical variables such as structural coupling (or disk participation) on the one hand, and mistuning sensitivity on the other. A thorough discussion is presented in later sections on how tuned vibration characteristics relate to disk participation and structural coupling.

It is also known [12] that for weakly coupled structures mode localization is proportional to the modal density. However, it was established by the same authors that this is only a *necessary, but insufficient* requirement for large increases in the forced response. Indeed it was observed that severe mode localization could take place at regions of high modal density, yet in the absence of veering the forced response amplification can very well be low. On the other hand, with the presence of veering, even at a 'far distance' from the point of operation, a noticeable increase in the mistuned response is commonly observed. For example, consider a mode set to which a group of excited mistuned modes belong. If the loci of this set veers away at any point, then these excited modes will experience higher amplifications compared to those of a set in which veering does not take place. Therefore, another important physical argument revolves around the influence curve veerings have on producing excessive vibrations regardless of the level of tuned system structural coupling at the point of excitation. The relationship between mistuning sensitivity and the degree of mistuning, at the various conditions, is yet another matter of high significance. More discussions on these issues, among others, are included throughout this study.

A brief description of the ROM technique and the bladed disk model used in this work is presented in Section 2 to follow. Sections 3 and 4 cover the tuned free vibration characteristics, and the corresponding mistuned forced response, respectively. Section 5 presents, in detail, the correlations observed. This is followed by a comprehensive discussion in Section 6. Section 6 also includes a general set of graphically presented guidelines that serve as an inexpensive design tool for early assessments of mistuning sensitivity. Finally, the conclusions are drawn in Section 7.

2. Vibration Analysis of a Bladed Disk

A reduced order modeling technique originally developed by Castanier *et al.* [15] and Kruse and Pierre [16], and recently extended by Bladh *et al.* [14] is used in this study to obtain the mistuned forced response data. The technique produces ROMs of turbomachinery rotors directly from their finite element models (FEMs) in a systematic fashion. The process involves a component mode analysis of the rotor, with a truncated number of modal amplitudes describing the response of the assembly. Furthermore, the method utilizes cyclic symmetry. Thus only a single sector (Figure 1b) of the bladed disk is modeled rather than modeling the entire assembly (Figure 1a). Blade mistuning is introduced to the FEM by varying the Young's modulus, E, in the blade elements by a random variable δ:

$$E_n = (1+\delta_n)E_o, \quad n = 1, \ldots, N, \tag{1}$$

where n is the blade number and N is the total number of blades in the assembly. To account for the random nature of blade mistuning statistical analyses, utilizing Weibull distributions, are imbedded in the technique. The principal advantage of the reduced order modeling method is the considerable computational savings associated with solving for the dynamics response of an entire mistuned bladed disk with a reduced set of degrees of freedom. The research code that implements the above ROM technique is called *REDUCE*. The reader is referred to [14] for the full mathematical formulations.

The bladed disk analyzed is an industrial 29-blade rotor (Figure 1) which forms the second stage of a four-drum compressor rotor used in an advanced gas turbine application. In this design, the blades and disk are machined from a single, continuous piece of material. Such design is referred to as a blisk. The material properties for the model are listed in Table 1. The single sector model in Figure 1b represents the tuned finite element model, with cyclic symmetry constraints imposed on the disk sector-to-sector boundaries. The model is clamped at the outward rims, which is a rough approximation of boundary conditions due to adjacent rotor stages. The sector finite element model is constructed with linear brick elements (eight-noded solids). The disk portion of the model contains 528 elements, and the blade portion has 375 elements. There are 4374 independent degrees of freedom in the single-sector finite element model.

Material Property	Property Value
Modulus of Elasticity, E_0	29.5 $(10)^6$ *psi*
Modulus of Rigidity, G	11.3 $(10)^6$ *psi*
Mass Density, ρ	7.40 $(10)^{-4}$ $lbsec^2/in^4$
Poisson's Ratio, ν	0.305
Structural Damping, γ	0.006

Table 1. Blisk material properties

3. Tuned Free Vibration Characteristics

The free vibration characteristics of a tuned bladed disk are best presented through a diagram of natural frequencies versus number of nodal diameters. Figure 2 shows this diagram for the bladed disk under investigation. Note that the method of Bladh *et al.* [14], which was referred to in Section 1, is used to obtain continuous plots of the eigenfrequency versus the number of nodal diameters. The diagram exhibits two interesting features that are common for most tuned rotor models. First, the disk stiffens rapidly as the number of nodal diameters increases due to increased disk waviness. It is therefore deduced that modes on highly slanted lines in Figure 2 correspond to disk-dominated modes. In contrast, blades do not stiffen significantly as the number of nodal diameters increases. Hence, modes on lines that are approximately horizontal represent families of blade-dominated modes. Modes on lines that are slightly slanted are 'mixed' modes, i.e., modes with both disk and blade contributions. It is hypothesized that without much disk motion, the blades vibrate in isolation. Thus, low and high relative disk participation is associated with weak and strong structural interblade coupling, respectively. This description explains the relation (referred to in Section 1) between the slope of the eigenfrequency loci on the one hand and the relative level of disk participation, and hence structural interblade coupling, on the other. A description of the character of each family of blade-dominated modes is given and denoted by a short code on the far right side of Figure 2.

A second notable feature in Figure 2 is the numerous eigenfrequency veerings referred to in Section 1. These involve blade- and disk-dominated mode families that veer away from each other. Attention is focused on five distinct eigenfrequency veerings labeled P through T. The mode sets (eigenfrequency loci) involved in these veerings are labeled A through H. For instance, with the above denotation, the eigenfrequency loci of Mode Set A consists of a first (lowest) torsion (1T) blade-dominated mode at zero nodal diameter. The set then transforms as the number of nodal diameters increases into one that is disk-dominated (1^{st} disk mode). Following this, the set veers away from the loci of Mode Set B, and transforms back to a blade-dominated type. After this transition, Mode Set A becomes dominated by the 'second blade bending about the weak axis' mode (2W). This eigenvector transition that takes place at the veering is one of the remarkable outcomes associated with curve veerings [17].

An important characteristic of a veering is its sharpness. The sharpness of each of the veerings is purely a tuned system characteristic. It is realized that at a veering the energy of a mode set transforms from one type of mechanism to another, e.g., from 1^{st} disk mode dominance to 2W blade mode dominance at Veering P. Hence it can be deduced that the sharpness of a veering depends on the degree of 'compatibility' between the two mode types involved. In fact, it is observed that most of the veerings incorporating the 1^{st} disk mode are relatively sharp compared to those involving the 2^{nd} disk mode (2^{nd} highly slanted line to the left). If an operating point coincides with a veering region, the degree of veering sharpness could be related to disk participation, and, in turn, structural interblade coupling as explained above. In a sharp veering mode transformation takes place swiftly (with a varying interblade phase angle), and within the veering there is a small region where the eigenfrequency line is slanted. In contrast, in a smooth veering mode transformation takes place gradually, and within the veering there is a large region where the eigenfrequency line is slanted (i.e., a large region where the relative level of disk participation is significant). Recalling the previously mentioned relationship between disk participation and structural interblade coupling, it can be concluded that sharp veerings are associated with weak coupling; and that smooth veerings are associated with stronger coupling.

In this study, the tuned free vibration characteristics are defined by the following three distinct variables:

1. The slope of the eigenfrequency loci. This can easily be measured at all regions of the eigenfrequency versus number of nodal diameters plot except within the neighborhood of veerings.

2. The finite difference curvature of the eigen-frequency loci veerings. The maximum range of curvature at a veering is used as an indication of veering sharpness.

3. The minimum eigenfrequency separation, in kHz, between mode sets at the veering.

Figure 3 graphically demonstrates the definition of each of these tuned free vibration characteristics. Figures 4 through 13 respectively show the veering curvatures, and the minimum eigenfrequency loci separations corresponding to Veerings P through T. The curvatures are computed using a standard fourth-order finite difference scheme.

4. Mistuned System Forced Response

In this section the forced response of the mistuned system is considered at a wide range of operating points. At the overall assembly level, a bladed disk can be excited in a manner such that a certain number of nodal diameters appear in the response configuration. This is referred to as engine order excitation (EOE). As mentioned earlier the blisk under investigation has 29 blades. Therefore, the response under values of EOE ranging from 0 to 14 (assembly's range of harmonics) is computed in order to examine the role of 'distance from veering' vis-à-vis mistuning sensitivity. At the blade level, a single harmonic point load is applied at the tip and mid-chord of each blade, normal to the local surface of the blade. All forced response data presented in this section are obtained utilizing the first five disk modes and the first ten blade modes. Furthermore, the statistical analyses are based on a total of 50 realizations, in which a different mistuning pattern is used for each realization. The degree of mistuning is expressed as a percentage value.

It should be noticed that the eigenfrequency versus number of nodal diameters representation ceases to be valid once mistuning is introduced to the system. The mode pairs of a particular mode family spread in the frequency domain as a result of mistuning, and, unless the degree of mistuning is very week, nodal lines across the disk no longer become distinctly apparent. An EOE of any value will inevitably excite the entire range of modes that lie within the frequency band of excitation. Naturally, some modes will receive more of the excitation energy than others depending on the location of the operating point. It is assumed that the closer the EOE is to the original 'tuned' location of the excited mistuned mode, the more this mode will get excited.

The mistuned forced response at frequency ranges in which the blade mode contribution arises from the 2W (2^{nd} blade bending mode), 2T/2W (combination of 2^{nd} blade bending and 2^{nd} blade torsion modes), 2T and 3W mode families is considered. The variation of the maximum mistuned forced response (among all 29 blades) versus degree of mistuning for the different values of EOE is presented in Figures 14 through 17, respectively, for each of these four mode families. In these figures, the 99.9 percentile values of the statistical response distributions are plotted. Note that the mistuned response is normalized with respect to the response of the tuned state, hence the term, 'mistuned response amplification'. The variation of the highest value (among all mistuning cases) of the maximum response amplification is shown versus EOE for the same families in Figures 18 through 21, respectively.

Consider an arbitrary curve among the mistuned response amplification versus percentage mistuning curves presented in Figures 14 through 17. Note that with the introduction of a small amount of mistuning, the response rapidly increases in magnitude. This, as explained in Section 1, is attributed to the fact that any level of disorder in a periodic structure leads to inhibiting the even distribution of vibration energy. This in turn leads to significant vibrations at certain blades due to localization. Interestingly, however, the mistuned response amplification reaches a peak at a certain value of mistuning, then reduces in magnitude and levels off at high values. The reason behind the reduction, and subsequent asymptotic leveling, relates to the fact that the participation factors of the mistuned modes become more evenly distributed as mistuning increases. This results in reducing the value of the EOE modal force, hence a reduction in the maximum mistuned response.

The intermediate degree of mistuning with which the maximum forced response is associated will be denoted *critical mistuning*. Consider the linear slope of the response amplification curve versus percentage mistuning, at low values of mistuning. It is observed that in most cases when the slope is steep, the critical mistuning value is low, and vice versa. The response amplification slope at low mistuning is therefore a good indication of critical mistuning. Let this slope be denoted as the *amplification-mistuning slope*. Figures 22 through 25 respectively show the amplification-mistuning slopes for the four mode families considered.

5. Correlations Between Tuned Free Vibration Characteristics and Mistuning Sensitivity

MS of a non-veering mode set

It is well known [12] that for weakly coupled structures mode localization is proportional to the modal density. Based on previous discussion, blade-dominated modes are generally associated with weak structural interblade coupling. Furthermore, it is known that any level of disorder, i.e. mistuning, causes a repeated mode to divide into a multiple set of close modes. The higher the mistuning is, the more scattered the frequencies of the modes are, which in turn means lower modal density. It is therefore reasonable to assume that severe mode localization is likely to occur when a blade-dominated mode family of a moderately mistuned system is excited. As an example, consider the 1W blade mode family shown in Figure 2. The behavior of this mode family was

examined in [18] for a rotor very similar to the one analyzed in this study. It was observed that indeed there was severe mode localization when typical densely located mistuned modes of this family were excited. Interestingly, however, it was shown that the set experienced only moderate (~5%) amplitude magnifications. It was therefore established that high modal density in a weakly coupled system is only a *necessary, but insufficient* requirement for large increases in the forced response. It is of interest to note that the loci of this 1W mode set does not veer away at any point. Let a set of this type be referred to as a *non-veering mode set.*

MS versus structural interblade coupling

In addition to the level of modal density, another factor that influences the mistuned response is the structural interblade coupling as demonstrated in [12]. As mentioned earlier, the level of interblade coupling depends on both the structural characteristics and the operating point. If the excited modes belong to a set that has a horizontal eigenfrequency loci, then the relative level of disk participation is low, hence the coupling is weak. On the other extreme, disk dominated modes (i.e. highly slanted eigenfrequency loci) correspond to high structural interblade coupling. In between these two extremes, there are mixed modes, which are associated with intermediate levels of coupling.

Table 2 lists the values of maximum mistuned forced response amplifications for three different disk dominated modes that belong to the 1st disk mode set (see Figure 2). Figure 26 shows the variation of mistuning sensitivity with engine order excitation for the mixed 4W/1R mode family (see Figure 2). This family is chosen because the slope of its eigenfrequency loci, away from the veering, indicates mixed disk-blade participation. Here, the results are obtained utilizing 5 disk modes and 14 blade modes in the ROM model.

Disk mode	Amplification
Mode set B, ND 1	1.2019
Mode set C, ND 2	1.3604
Mode set F, ND 4	1.4714

Table 2. Maximum mistuned forced response amplifications for several disk-dominated modes. ND refers to 'nodal diameter'.

Note that the cases focused on here are ones where the modes in question are located 'far' away from any veerings in the eigenfrequency plot. It should also be noted that, unlike the cases of the previous subsection, all these modes belong to sets that veer away at some point. It is observed that the amplifications (~10% to ~50%) of all modes considered in Table 2 and Figure 26 are moderate, yet higher than those of the non-veering set modes examined in the previous subsection. A possible explanation refers to the relationship between curve veerings and MS. There are repeated observations in the literature that affirm that modes close to veerings are highly sensitive to mistuning. Whenever any mistuned mode pair of a veering set gets excited, sensitive modes that are originally close to the veering (i.e., in the tuned case) get excited as well. This contributes to the increase in the response. The importance of how 'close' excited modes are from a veering will be elaborated upon in the next sub-section.

It is noticed, from Figure 26, that there is an intermediate region (where the eigenfrequency loci slope is intermediate) of relative disk participation where the mistuned forced response peaks. Specifically, this region corresponds to EOE=8. This verifies results presented in the literature since, as mentioned earlier, the relative level of disk participation is directly proportional to interblade structural coupling. In other words this is consistent with the hypothesis that states that the maximum MS is associated with a 'critical' value of intermediate structural interblade coupling. Let this hypothesis be referred to as the *critical coupling hypothesis.*

Another interesting observation regarding modes that are 'far' away from veerings is the slight jump in amplification that appears at high values of EOE (clearly shown in Figures 18 through 21). This may be attributed to the fact that regardless of the slope of the eigenfrequency loci, structural interblade coupling is also related to the number of nodal diameters. As the number of nodal diameters increases, the disk becomes more 'rigid-like'. This results in a lower level of interblade coupling since the avenue of vibration transmission via the disk is reduced. Based on this description, a response peak (these jumps at high EOE) is associated with an intermediate level of structural interblade coupling. Again, this validates the critical coupling hypothesis.

MS versus 'distance from veering'

It is instantly noticed from the mistuned forced response diagrams (Figures 14 through 21) that the highest values of maximum amplification occur in regions close to veerings. The eigenfrequency veering is essentially a region where the loci of disk- and blade-dominated modes veer away from each other. It could therefore be assumed that at the exact center of a veering, modes are almost equally mixed in disk and blade participation. With such

Veering label	P	Q	R	S	T
Veering disk family	1st	1st	2nd	2nd	3rd
Veering blade family	2W	2T/2W	2T	3W	3W
Nodal diameter of considered mode pair	1	2	2	3	2
Maximum curvature range	12.83	6.70	4.83	3.31	3.28
Minimum eigenfrequency separation [kHz]	0.35	0.80	1.35	1.05	0.74
Maximum amplification	*2.143*	*2.705*	*2.863*	*2.791*	*2.667*
Mistuning level associated with maximum amplification [%]	0.8	2.5	3	2.5	1.7
Slope of max. amplification versus mistuning, at low mistuning	556.9	465.6	431.8	376.1	404.1

Table 3. Tuned vibration characteristics and corresponding mistuning sensitivity information for curve veerings P, Q, R, S, and T (see Figure 2). The last two rows refer to the critical mistuning and the amplification-mistuning slope, respectively. Note that the highest maximum amplification is associated with veering R.

significant level of disk participation the structural interblade coupling is assumed to be relatively high. As the distance along the nodal diameter axis from the veering increases, the more blade-dominated the modes become and hence the weaker the coupling.

To check the validity of the critical coupling hypothesis in this context (i.e., effect of the 'distance from veering'), a new set of similar bladed disk models are constructed with varying disk properties. The purpose of this is to create cases where the curve veering under examination is located at different locations across the number of nodal diameters axis. The variation of the disk stiffness leads to a change in the location of the veering from the value of applied engine order excitation. This is an indirect way of examining the influence the 'distance from veering' has on MS. Figure 27 shows the eigenfrequency loci for values of disk stiffness varying from 90% to 110% of some nominal value. Note the shifting of the 'center' of the curve veering. A stiffness value of E≈91% corresponds to the case where the 2nd nodal diameter (value of the applied EOE) lies exactly at the 'center' of the veering. Figure 28 shows the relationship between MS and the value of disk flexibility, which, as mentioned above, reflects the relationship between MS and the nodal diameter distance between the value of EOE and the veering. Both Figures 27 and 28 are obtained from the literature [19]. It is noticed that the mistuned forced response amplification has a local minimum at the 'center' of the veering. This result proves that at the exact 'center' of a veering the relative level of disk motion is much higher than the level required in the critical case. More importantly, it is observed that a maximum value of MS is associated with a certain nodal diameter distance from the veering, as would have been predicted by the critical coupling hypothesis. The precise level of structural interblade coupling at this distance is the critical level. Associated with this level is a delicate balance of disk and blade participation.

MS versus veering characteristics

Consider the cases where the EOE is at, or close to, the actual veering region. Here, as shown in Figure 14 through 17, the mistuned response amplification is bound to be most severe. This is because most of the excitation energy (due to the closeness of the value of EOE) works on exciting the modes that are at the veering, which commonly are critically coupled, or at least close to such. In this context, the characteristics of the eigenfrequency veering are expected to clearly correlate with the extent of mistuning sensitivity. The five veerings labeled P through T in Figure 2 are considered. Table 3 summarizes the relationship between the characteristics of these veerings and the corresponding amplitudes of the mistuned response amplification. It is noticed that there is an intermediate level of veering curvature with which maximum MS is associated. Namely, Veering R has this critical curvature (4.83). In reference to the critical coupling hypothesis, it can be deduced that the level of structural interblade coupling

corresponding to the tuned mode pair that lies at the edge of Veering R is the critical level (in comparison to the levels associated with the other considered veerings). Table 3 also shows the relationship between MS and yet another veering characteristic: the minimum eigenfrequency distance at the veering. The results show that this minimum veering separation distance is highest for Veering R, the veering associated with the critical MS. This observation, if proven to be generally true, will render the minimum veering separation distance a simple and straightforward indication of MS.

MS versus degree of mistuning

Table 3 also shows the mistuning level responsible for the maximum MS (i.e. critical mistuning) corresponding to Veerings P through T. Upon comparing the values of critical mistuning for the veerings, it is noticed that this quantity peaks (3%) for the critically coupled case associated with Veering R. This result implies that the closer the structural interblade coupling is to the critical level, the higher the degree of mistuning needed to cause maximum MS. Furthermore it is noticed that the amplification-mistuning slope for Veering R is relatively low (the lowest slope is that of Veering S). This, to a certain extent, confirms that the value of critical mistuning is inversely proportional to the amplification-mistuning slope.

6. Discussion

Summary of factors that contribute to mistuning sensitivity

The results presented confirm that there is a critical degree of structural interblade coupling at which MS is maximized. The effect of critical coupling is additive to that of the existence of high modal density. Physically it is conceivable, and indeed proven in Figure 26, that associated with the critical coupling level there is a delicate balance of disk and blade participation. Hence, it can generally be viewed that structural interblade coupling and the relative level of disk participation are directly related. In fact, the former can be considered to be a consequence of the latter. It should be noticed that the coupling referred to here is a variable that changes with the state of operation. From a materials perspective, the structural interblade coupling depends on the properties of the disk-blade sector as well as that of the disk-blade interface. The level of operational (as opposed to material) structural interblade coupling depends on the tuned free vibration characteristics, as well as the operating conditions, through the following four factors:

1. Nodal diameter distance between veering and excited mode pair.

2. Curvature of veering at which an excited mode pair lies.

3. Slope of eigenfrequency loci to which an excited mode pair belong.

4. Value of nodal diameter (or EOE).

Based on the results presented, the above four factors are roughly ordered in descending order of significance with regards to the effect critical coupling has on increasing the MS. At this point, it is worth noting that such order may change from one model to another. The increase in MS is measured in comparison to the value of MS at a non-critically coupled state belonging to the same mode set. It is noticed that the degree of increase in MS associated with the combined effect of the first and second factors (~65% to ~110%) is commonly much higher than that is associated with the 3rd and 4th factors (~25% and ~10%, respectively). This is apparent from comparing the corresponding increases in mistuned forced response amplification. Data related to the 1st, 2nd and 4th factors is read from Figures 14 through 17; and data related to the 3rd factor is read from Figure 26. Note that curve veerings are the prime cause for major increases in MS. A candidate explanation for this is that whenever a mode pair that lies within, or close to, a veering gets excited, and mode localization takes place, a certain amount of disk vibrational energy gets *trapped* in the blades as energy gets transmitted from one blade to another via the disk. Perhaps this is a unique outcome that occurs for critically coupled states that are at, or close to, veerings. Recall that at a veering mode shape transformation takes place. The significant influence of curve veerings sheds light upon the importance of their detailed characteristics, and upon the relevance of how close a veering is to the EOE. With these factors considered, as well as the other coupling factors mentioned, there is clearly a substantial degree of complexity linked to the problem of predicting mistuning sensitivity of a bladed disk. Figure 29 qualitatively summarizes the effects of all the factors, including critical mistuning. Note that there is a 'critical' value associated with all the presented factors. Also included in Figure 29 is an abbreviated description of the underlying physical mechanisms that relate MS to structural interblade coupling.

General guidelines for bladed disk design

The most ambitious outcome of the analyses and insights presented in this paper would be a set of design guidelines for a mistuning-resistant turbomachinery rotor. Figure 30 presents a preliminary version of such guidelines. In particular, Figure 30 presents a schematic diagram that classifies the various operating zones, qualitatively, and indicates the corresponding 'anticipated' MS. The diagram is based on the results and analyses presented in this study, as well as some reported results from the literature. It is worth noting that the conclusions arrived at here are based on an integrated view of all the factors referred to in this study, and that the relative importance of these factors may differ from one physical model to another. With a minimum amount of reassuring forced response computations, the presented figure can be used as an inexpensive design tool for early assessments of mistuning sensitivity.

6. Conclusions

This paper focused on the analyses of the complex dynamic characteristics of an industrial bladed disk. The study explored the connection, and associated relationships, between the tuned free vibration characteristics and operating conditions on the one hand, and mistuning sensitivity on the other.

The characteristics of the eigenfrequency versus number of nodal diameters plot, supplemented with a recently published interblade phase angle representation, were used as the basis for quantifying the tuned free vibration characteristics. Furthermore, an advanced reduced order modeling technique was used as a tool to obtain a large set of mistuned forced response data. With the tuned free vibration characteristics quantified, and the mistuned response data in hand, a set of comprehensive correlative analyses was conducted and conclusions were derived.

It was concluded that there are numerous intertwining factors that affect mistuning sensitivity in a mistuned bladed disk. Most important is the structural interblade coupling that varies from an operating state to another. Results show that there is a critical value of coupling corresponding to maximum mistuning sensitivity. In addition, the influence of both the location and the characteristics of eigenfrequency veerings were proven to be of paramount importance. All the relevant factors were presented in connection to the eigenfrequency versus number of nodal diameters plot. Furthermore, the effects of these factors were presented quantitatively, and were thoroughly discussed from a physical perspective.

Finally, on the basis of the results and physical insights gained, a general set of guidelines was presented (in graphical form) as an inexpensive design tool for early assessments of mistuning sensitivity.

Acknowledgements

The authors gratefully acknowledge Dr. R. Bladh for providing several of the figures presented in this paper.

References

1. Anderson, P. W., 1958, "Absence of diffusion in certain random lattices," *Physical Review*, Vol. 109, pp. 1492-1505.
2. Montroll, E. W. and Potts, R. B., 1955, "Effects of defects on lattice vibrations," *Physical Review*, Vol. 100, pp. 525-543.
3. Robenstock, H. B. and McGill, R. E., 1968, "Vibrations of disordered solids," *Physical Review*, Vol. 176, pp. 1004-1014.
4. Ishii, K., 1973, "Localization of eigenvalues and transport phenomena in the one-dimensional disordered system," *Supplement of the Progress of Theoretical Physics*, Vol. 53, pp. 77-138.
5. Hodges, C. H., 1982, "Confinement of vibration by structural irregularity," *Journal of Sound and Vibrations*, Vol. 82(3), pp. 441-424.
6. Valero, N. A. and Bendiksen, O. O., 1986, "Vibration characteristics of mistuned shrouded blade assemblies," *ASME Journal of Engineering for Gas Turbines and Power*, Vol. 108(2), pp. 293-299.
7. Bendiksen, O. O., 1987, "Mode localization phenomena in large space structures," *AIAA Journal*, Vol. 25(9), pp. 1241-1248.
8. Pierre, C. and Dowell, E. H., 1987, "Localization of vibrations by structural irregularity," *Journal of Sound and Vibrations*, Vol. 114, pp. 549-564.
9. Pierre, C., Tang, D. M., and Dowell, E. H., 1987, "Localized vibrations of disordered multi-span beams: theory and experiment," *AIAA Journal*, Vol. 25(9), pp. 1249-1257.
10. Pierre, C., 1988, "Mode localization and eigenvalue loci veering phenomena in disordered structures," *Journal of Sound and Vibrations*, Vol. 126(3), pp. 485-502.
11. Pierre, C., 1990, "Weak and strong vibration localization in disordered structures: a statistical investigation," *Journal of Sound and Vibrations*, Vol. 139(1), pp. 111-132.

12. Óttarsson, G. S. and Pierre, C., 1995, "On the effects of interblade coupling on the statistics of maximum forced response amplitudes in mistuned bladed disks," in *Proceedings of the 36th AIAA/ASME Structures, Structural Dynamics, and Materials Conference,* New Orleans, Louisiana.
13. Bladh, R., Castanier, M. P., Pierre, C., 2000, "Component-mode-based reduced order modeling techniques for mistuned bladed disks, Part I: Theoretical models; and Part II: Application," *Proceedings of the 45th ASME Gas Turbine and Aeroengine Technical Congress, Exposition and Users Symposium,* Munich, Germany. Also, *ASME Journal of Engineering for Gas Turbines and Power*, in print.
14. Bladh, R., Pierre, C., Castanier, M. P., and Kruse, M. J., 1999, "Dynamic response predictions for a mistuned industrial turbomachinery rotor using reduced order modeling," *ASME Journal of Engineering for Gas Turbines and Power*, under review.
15. Castanier, M. P., Óttarsson, G., and Pierre, C., 1997, "A reduced-order modeling technique for mistuned bladed disks," *Journal of Vibration and Acoustics*, Vol. 119(3), pp. 439-447.
16. Kruse, M. J. and Pierre, C., 1996, "Forced response of mistuned bladed disks using reduce-order modeling," *Proceedings of the 37th AIAA/ASME Structures, Structural Dynamics, and Materials Conference*, Salt Lake City, Utah.
17. Perkins, N. C. and Mote Jr, C. D., 1986, "Comments on curve veering in eigenvalue problems," *Journal of Sound and Vibrations*, Vol. 106, pp. 451-463.
18. Bladh, R., Castanier, M. P., and Pierre, C., 1998, "Reduced order modeling and efficient forced response statistics prediction for mistuned bladed disks," *Proceedings of the 3rd National Turbine Engine High Cycle Fatigue Conference,* San Antonio, Texas.
19. Bladh, R., Castanier, M. P., and Pierre, C., 2001, "Effects of Multi-Stage Coupling and Disk Flexibility on Mistuned Bladed Disk Dynamics," *Proceedings of the 46th ASME Gas Turbine and Aeroengine Technical Congress, Exposition and Users Symposium,* New Orleans, Louisiana, to appear.

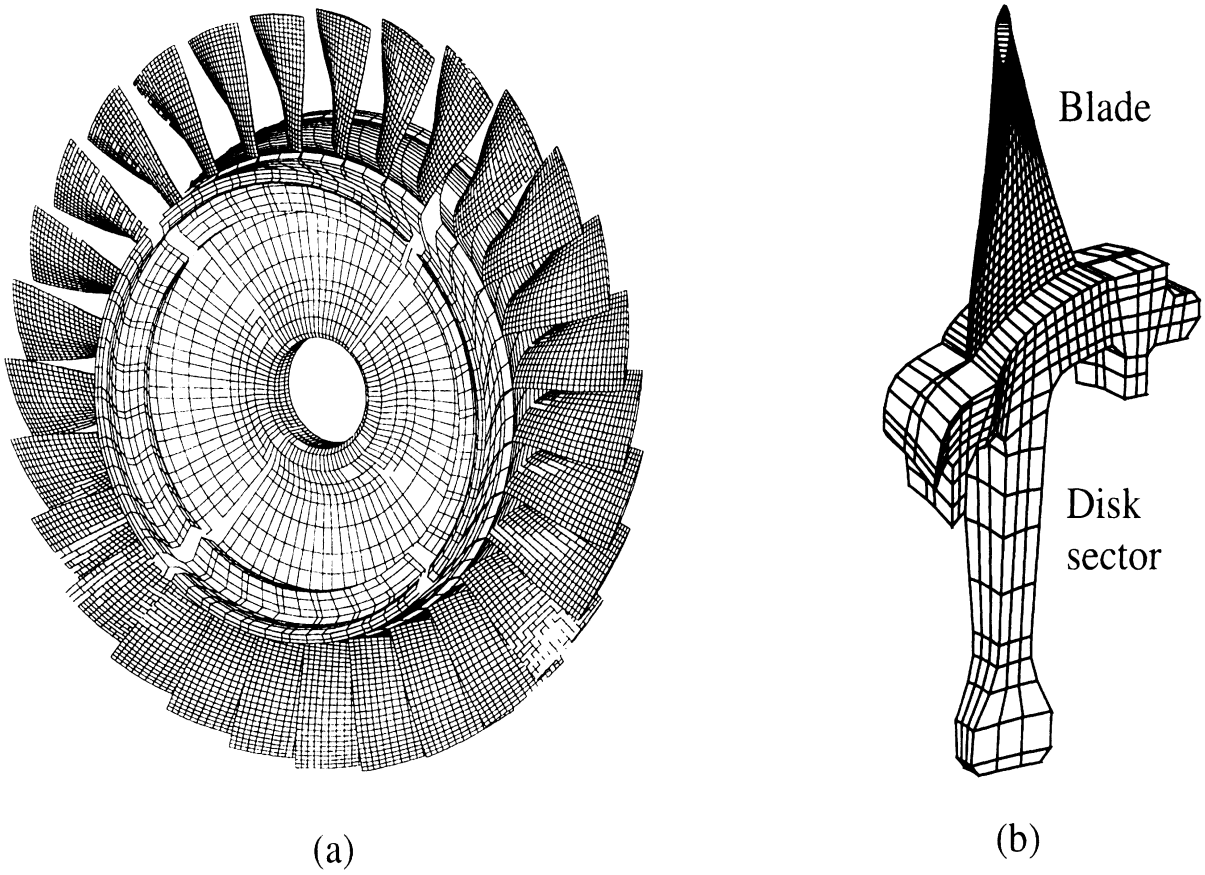

Figure 1. Finite element meshes for the industrial 29-blade compressor rotor: (a) full assembly model; (b) cyclic disk-blade sector model.

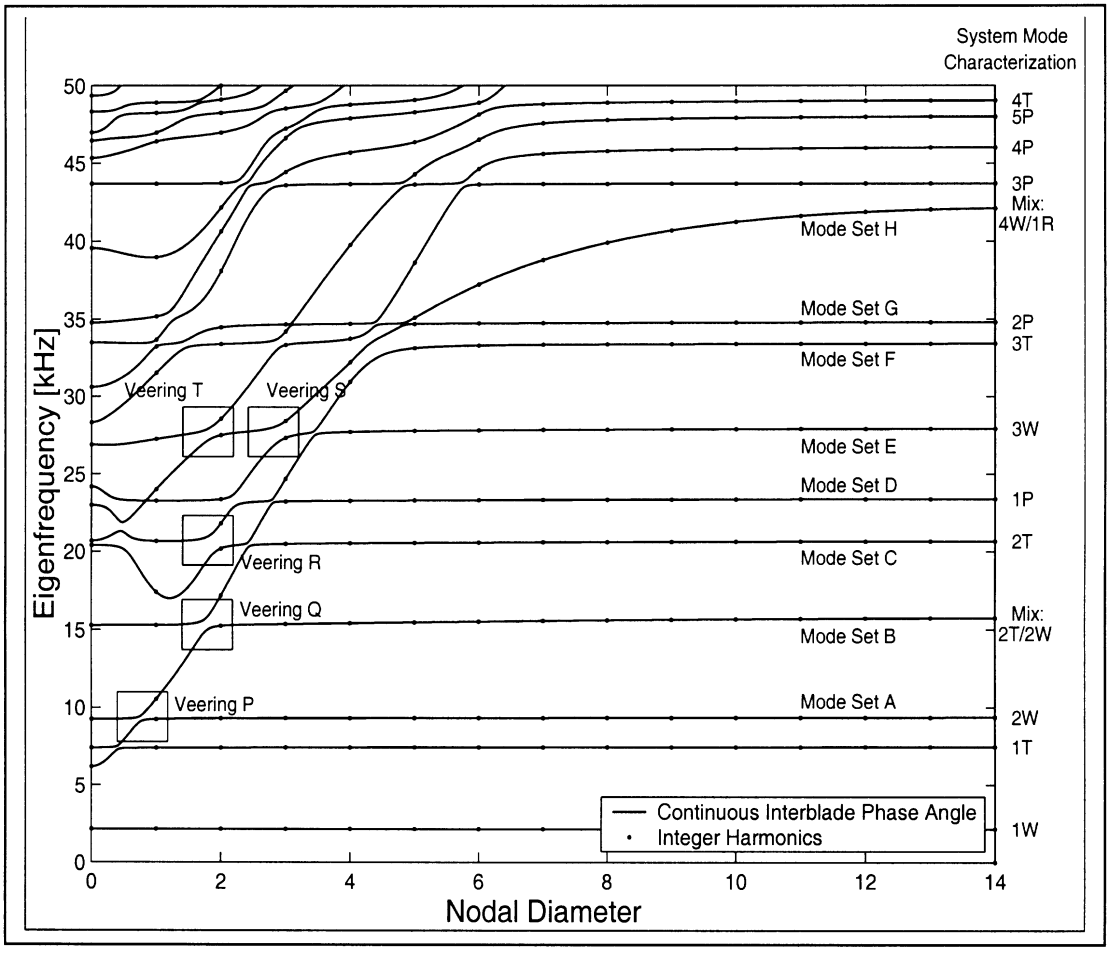

Figure 2. Natural frequencies versus number of nodal diameters for the tuned rotor. The character of each family of blade-dominated modes is indicated on the right, where W=Weak Axis Bending , T=Torsion, P=Plate, and R=Radial.

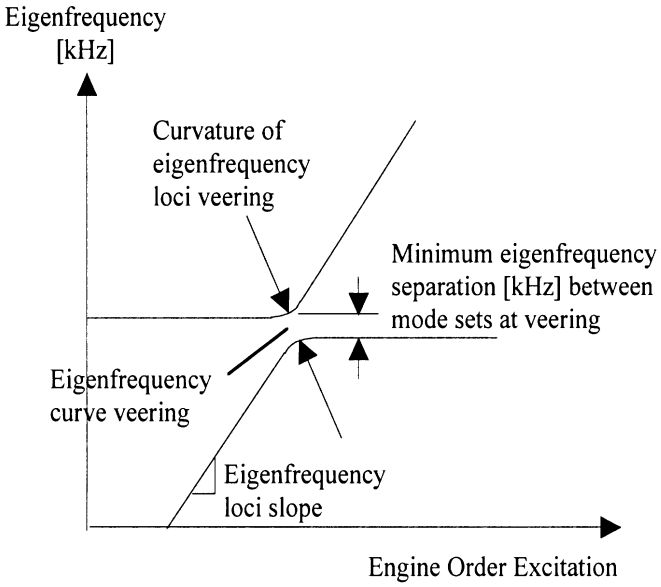

Figure 3. Geometric characteristics of curve veering.

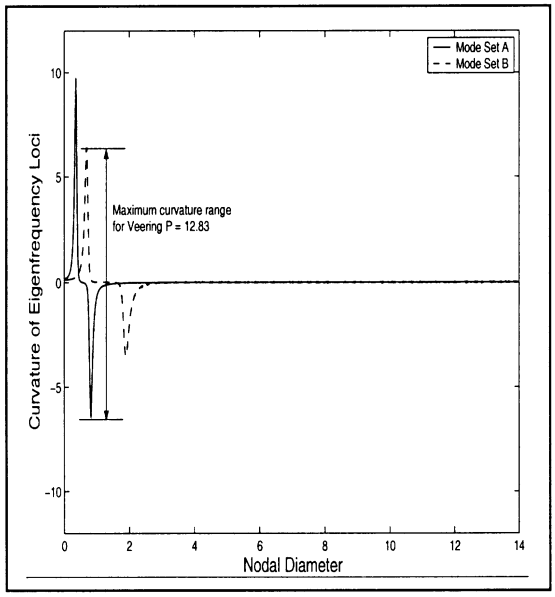

Figure 4. Finite difference curvature of the eigenfrequency loci for mode sets A and B.

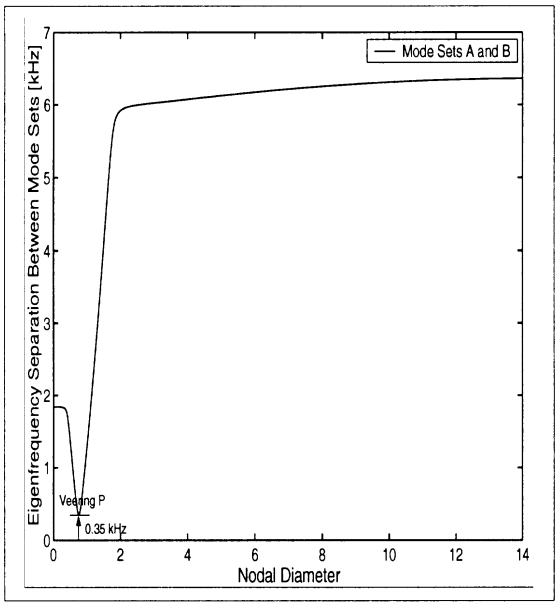

Figure 5. Eigenfrequency separation [kHz] between the eigenfrequency loci of mode sets A and B.

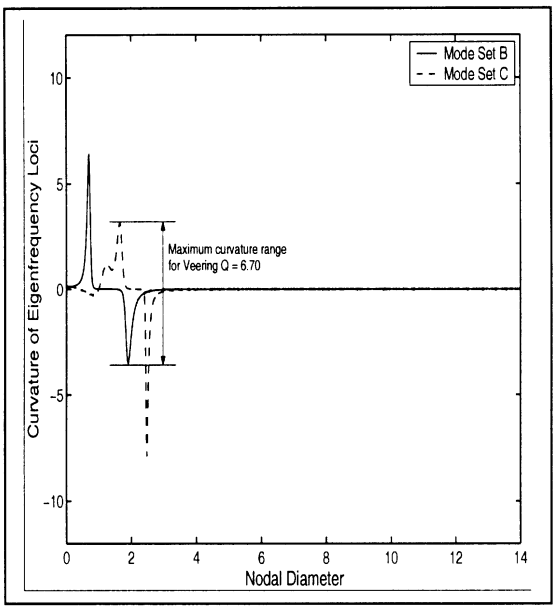

Figure 6. Finite difference curvature of the eigen-frequency loci for mode sets B and C.

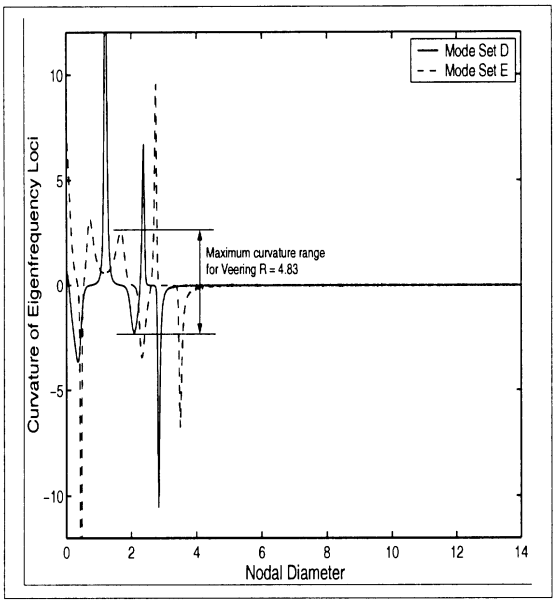

Figure 8. Finite difference curvature of the eigen-frequency loci for mode sets D and E.

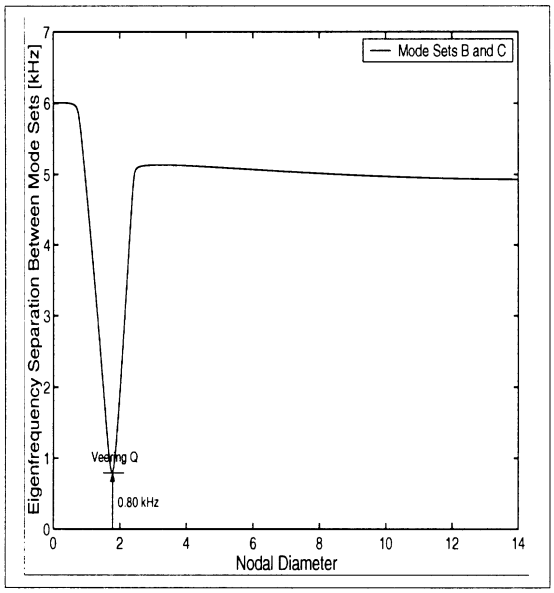

Figure 7. Eigenfrequency separation [kHz] between the eigenfrequency loci of mode sets B and C.

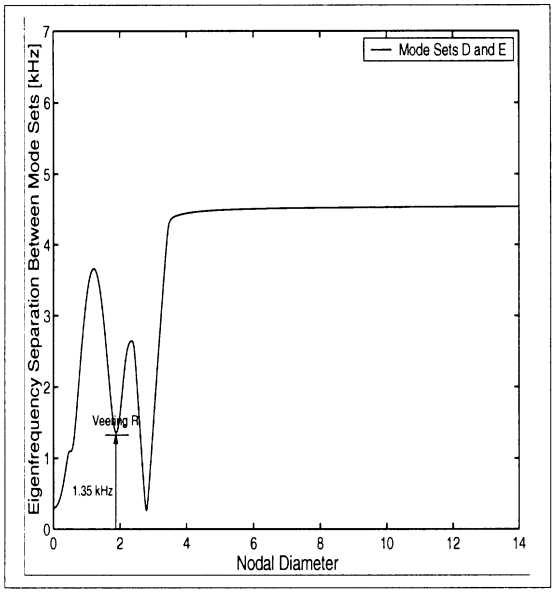

Figure 9. Eigenfrequency separation [kHz] between the eigenfrequency loci of mode sets D and E.

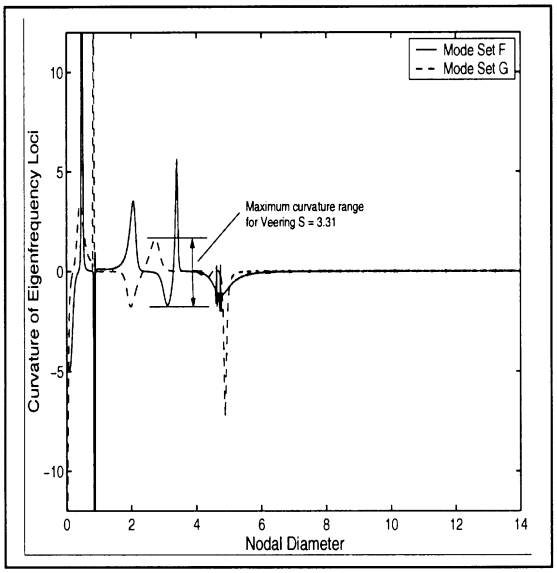

Figure 10. Finite difference curvature of the eigenfrequency loci for mode sets F and G.

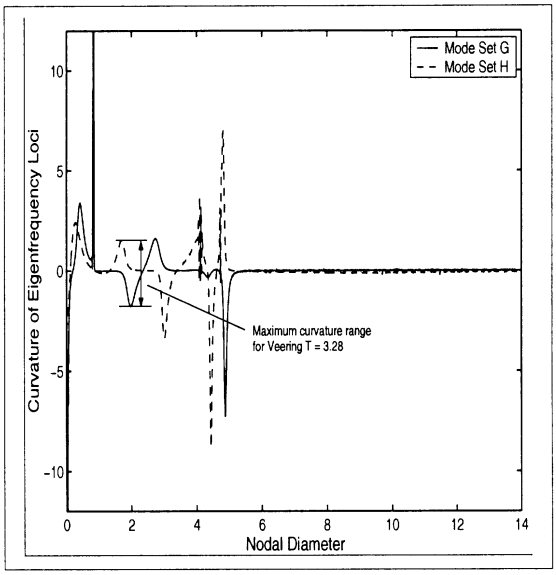

Figure 12. Finite difference curvature of the eigenfrequency loci for mode sets G and H.

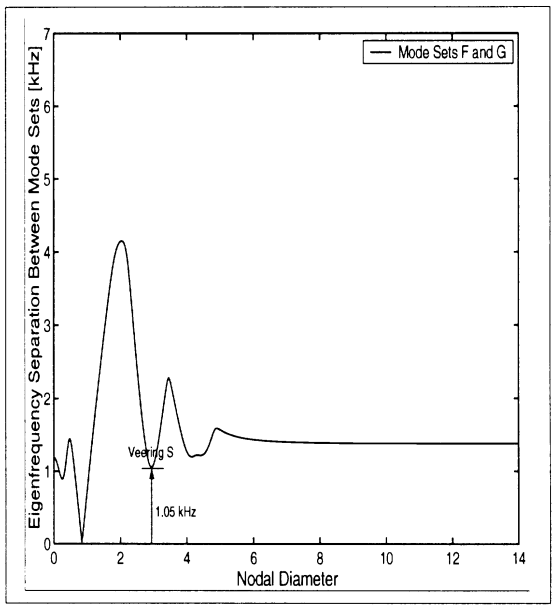

Figure 11. Eigenfrequency separation [kHz] between the eigenfrequency loci of mode sets F and G.

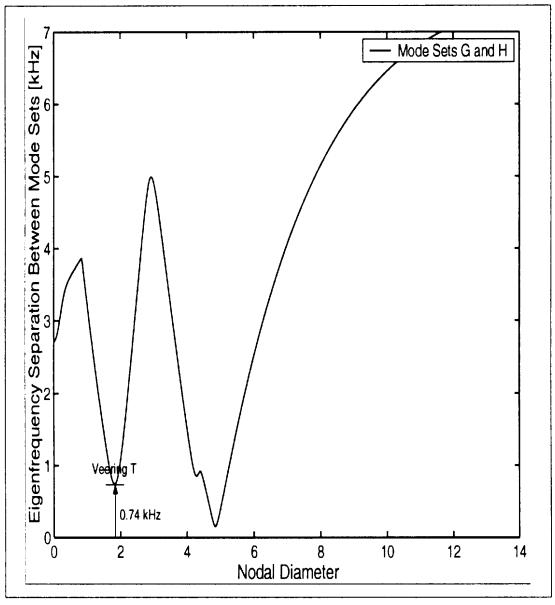

Figure 13. Eigenfrequency separation [kHz] between the eigenfrequency loci of mode sets G and H.

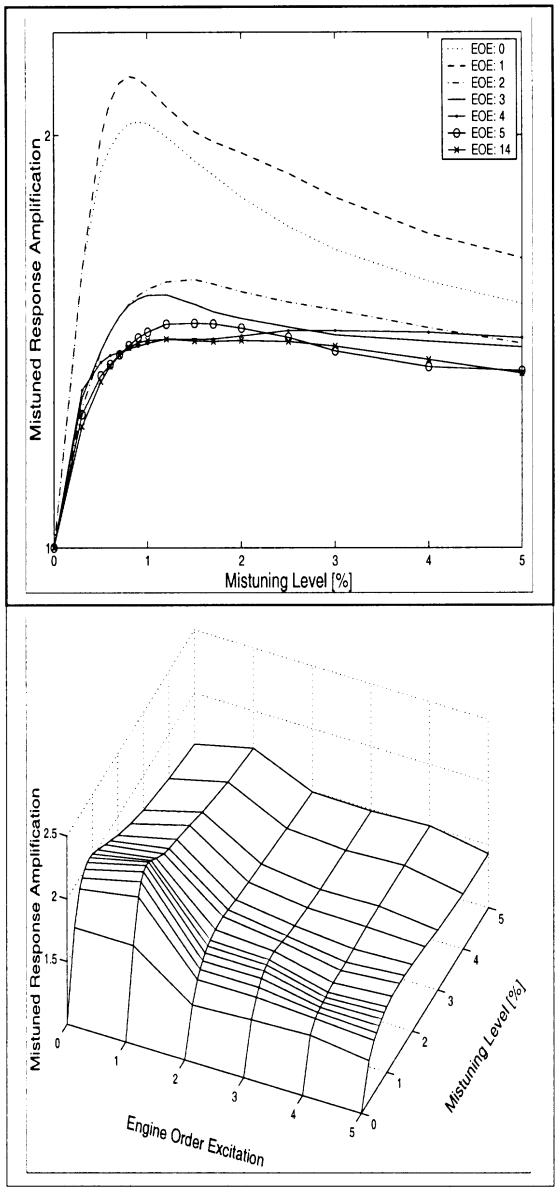

Figure 14a. Variation of maximum forced response amplification with the degree of mistuning for the 2W mode family at low values of engine order excitation.

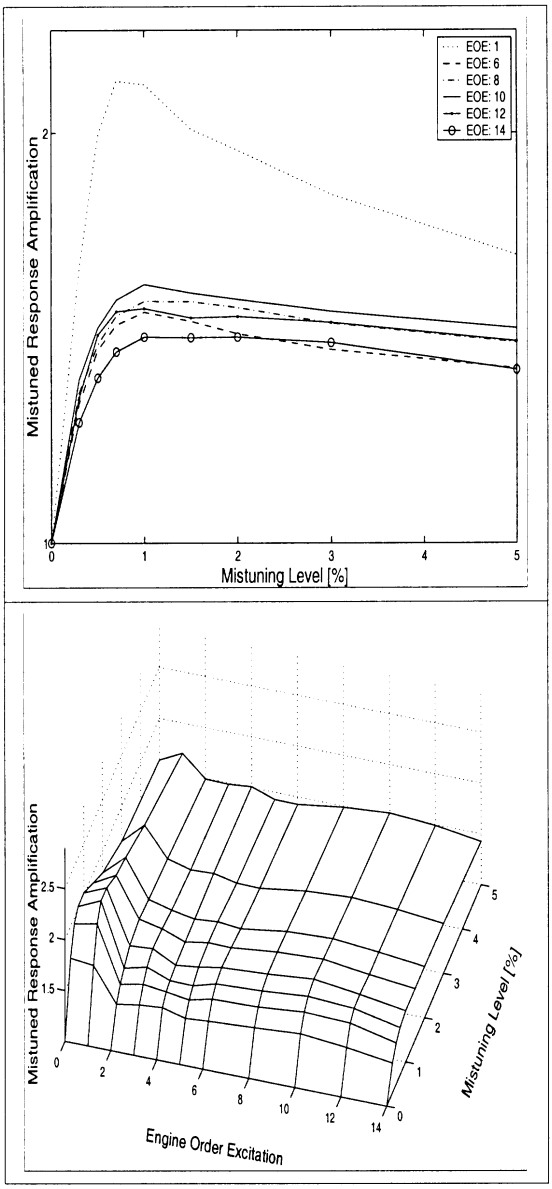

Figure 14b. Variation of maximum forced response amplification with the degree of mistuning for the 2W mode family spanning entire engine order excitation range.

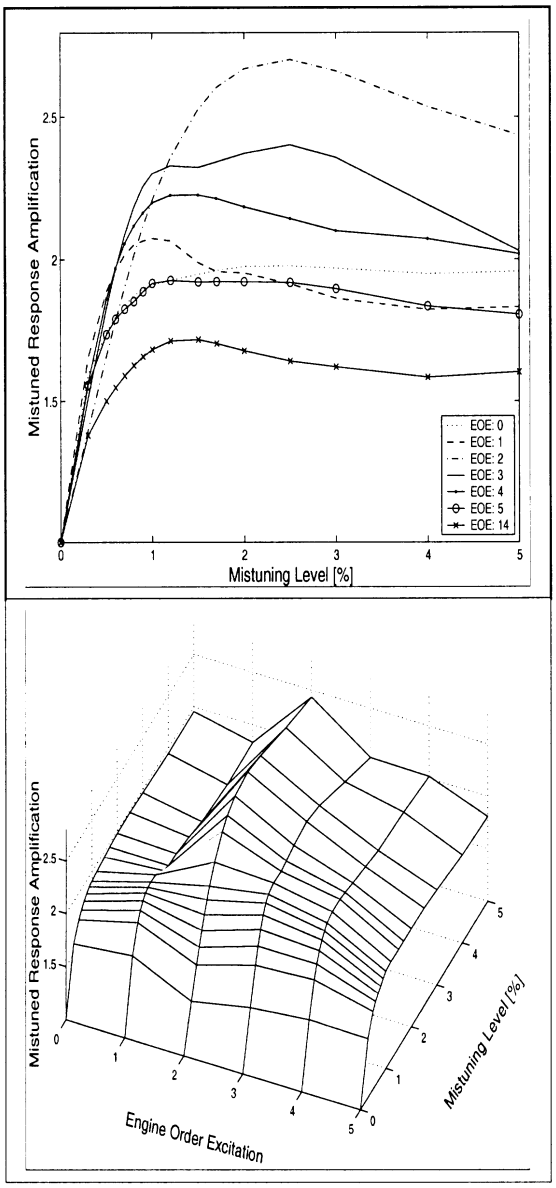

Figure 15a. Variation of maximum forced response amplification with the degree of mistuning for the 2T/2W mode family at low values of engine order excitation.

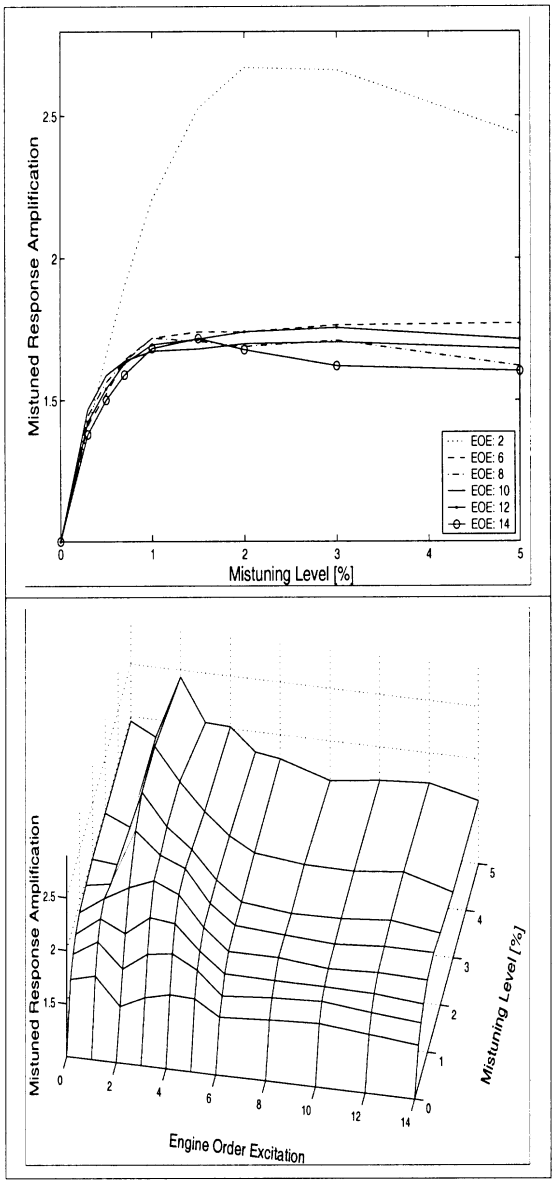

Figure 15b. Variation of maximum forced response amplification with the degree of mistuning for the 2T/2W mode family spanning entire engine order excitation range.

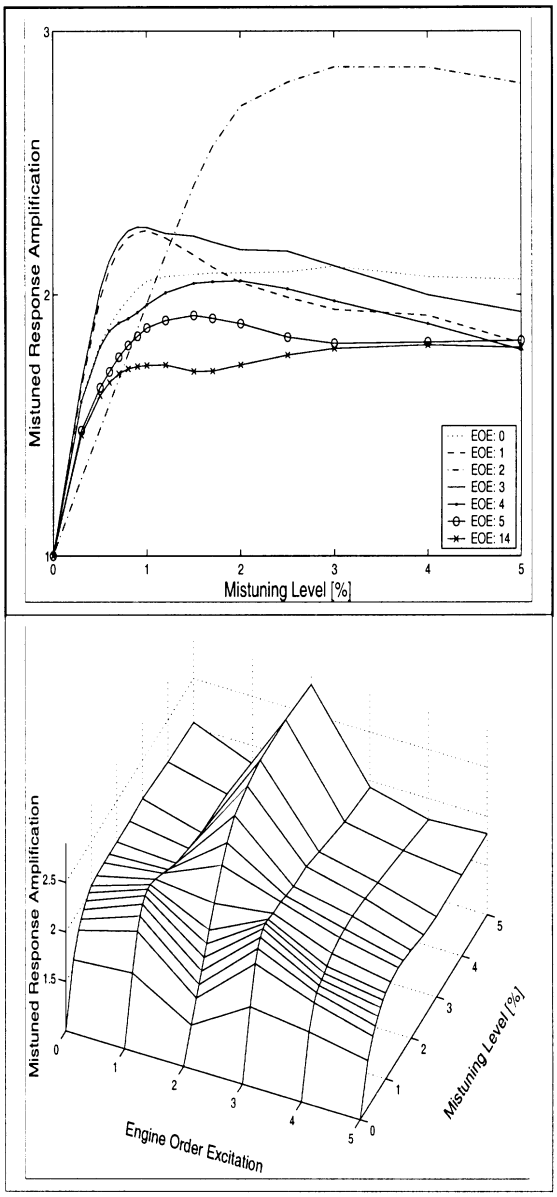

Figure 16a. Variation of maximum forced response amplification with the degree of mistuning for the 2T mode family at low values of engine order excitation.

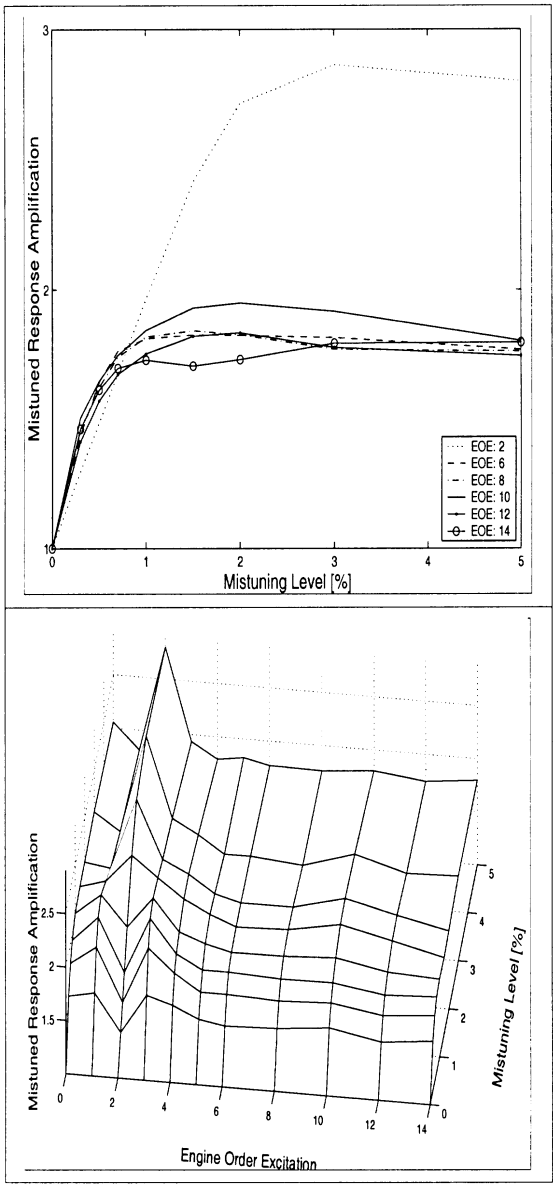

Figure 16b. Variation of maximum forced response amplification with the degree of mistuning for the 2T mode family spanning entire engine order excitation range.

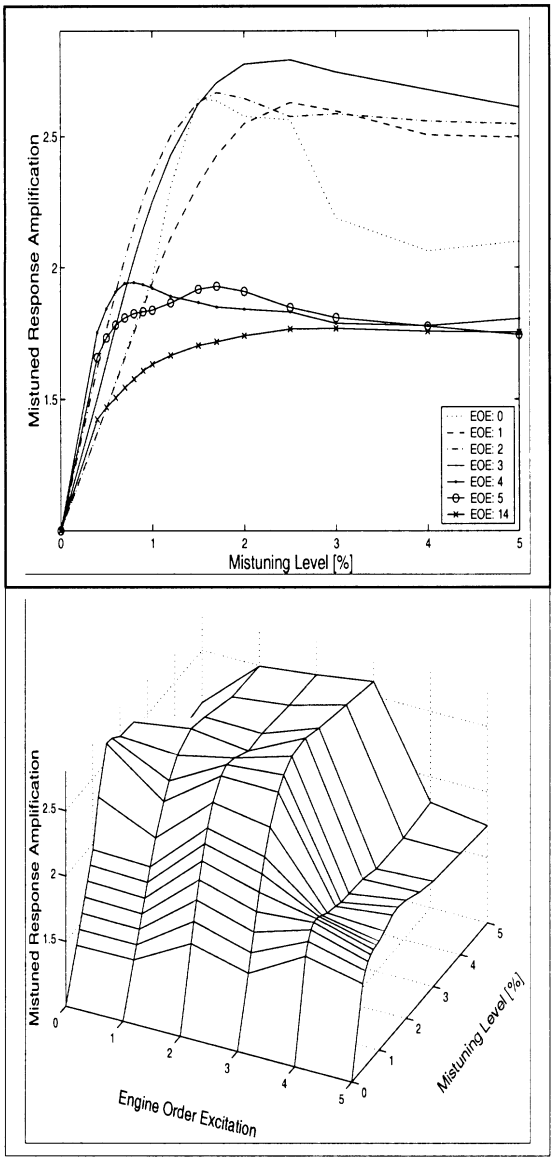

Figure 17a. Variation of maximum forced response amplification with the degree of mistuning for the 3W mode family at low values of engine order excitation.

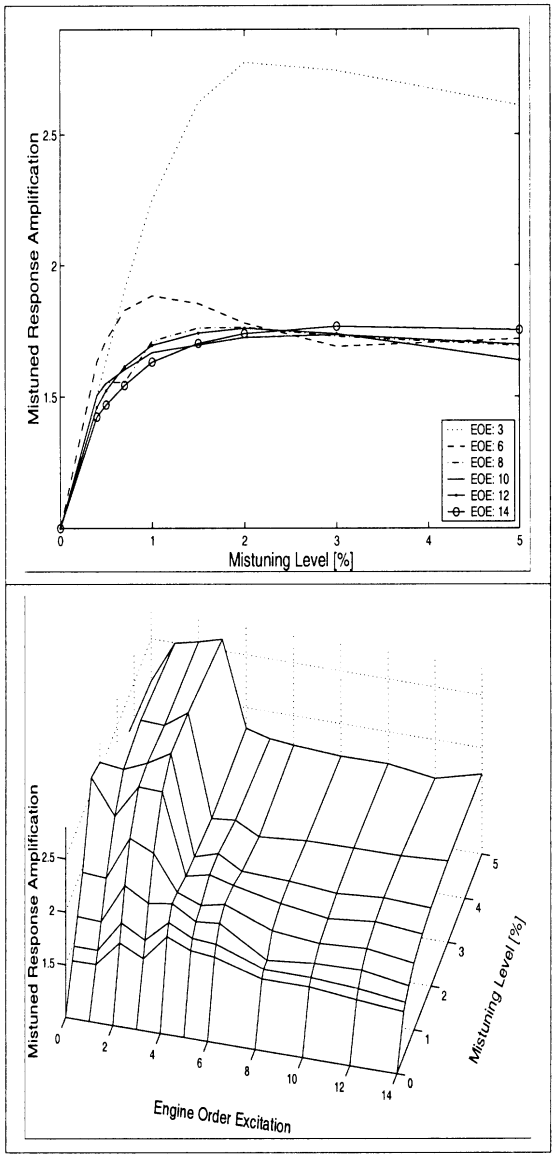

Figure 17b. Variation of maximum forced response amplification with the degree of mistuning for the 3W mode family spanning entire engine order excitation range.

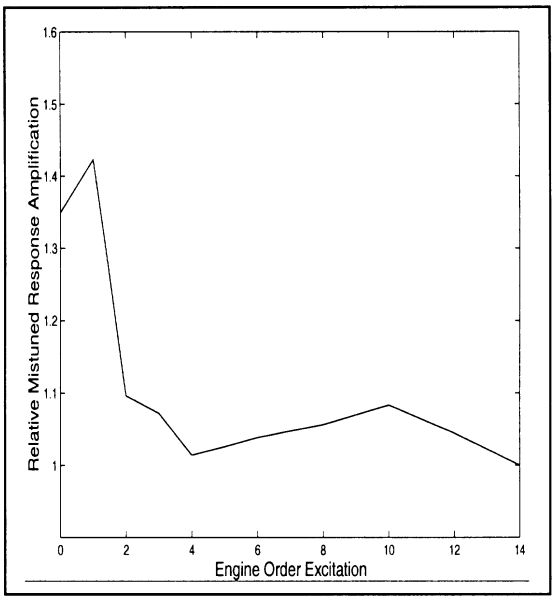

Figure 18. Variation of highest mistuned forced response amplification (among all mistuning cases) with engine order excitation for the 2W mode family. Here all data is normalized with respect the value of amplification at EOE 14.

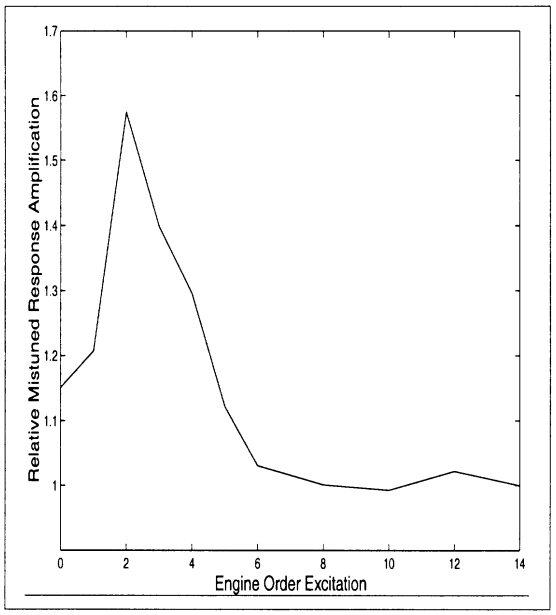

Figure 19. Variation of highest mistuned forced response amplification (among all mistuning cases) with engine order excitation for the 2T/2W mode family. Here all data is normalized with respect the value of amplification at EOE 14.

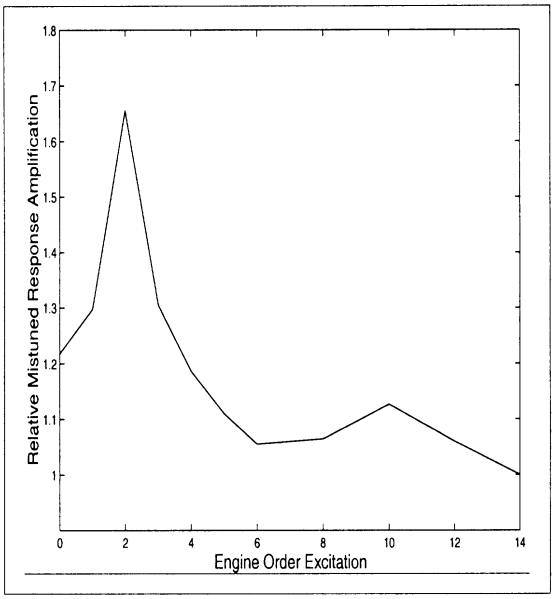

Figure 20. Variation of highest mistuned forced response amplification (among all mistuning cases) with engine order excitation for the 2T mode family. Here all data is normalized with respect the value of amplification at EOE 14.

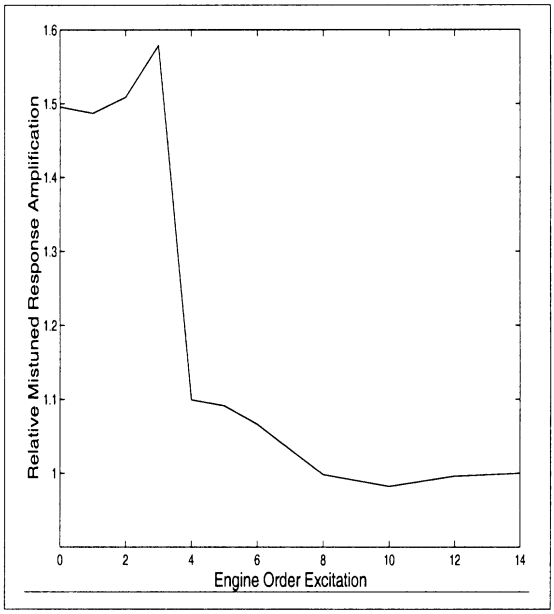

Figure 21. Variation of highest mistuned forced response amplification (among all mistuning cases) with engine order excitation for the 3W mode family. Here all data is normalized with respect the value of amplification at EOE 14.

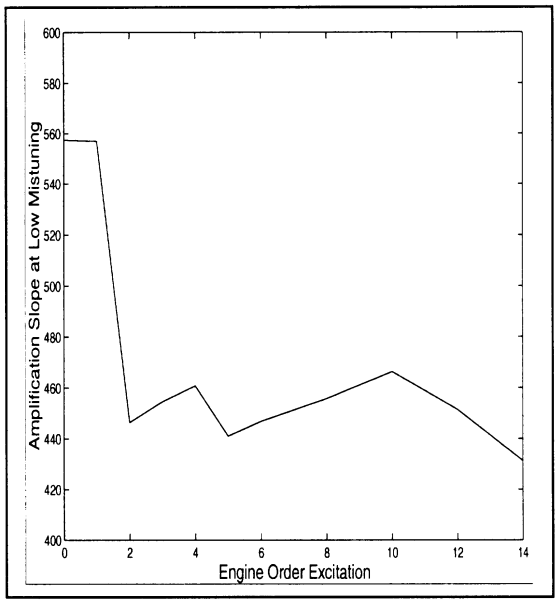

Figure 22. Variation of amplification-mistuning slope at low mistuning with engine order excitation for the 2W mode family.

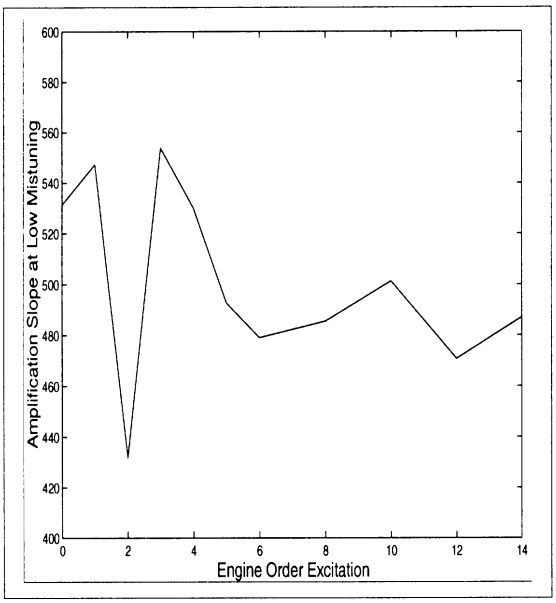

Figure 24. Variation of amplification-mistuning slope at low mistuning with engine order excitation for the 2T mode family.

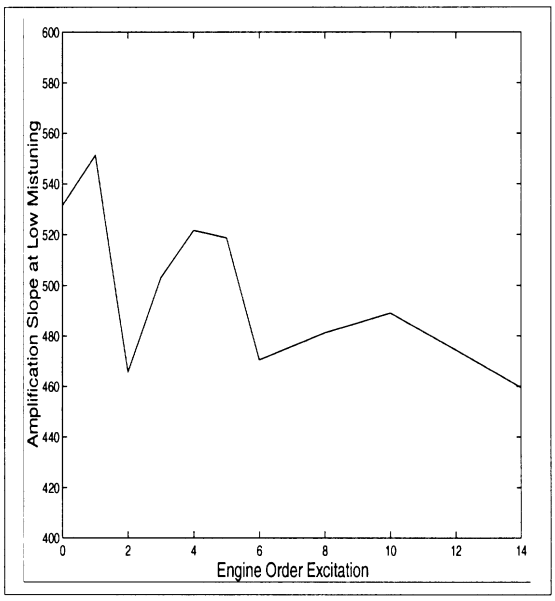

Figure 23. Variation of amplification-mistuning slope at low mistuning with engine order excitation for the 2T/2W mode family.

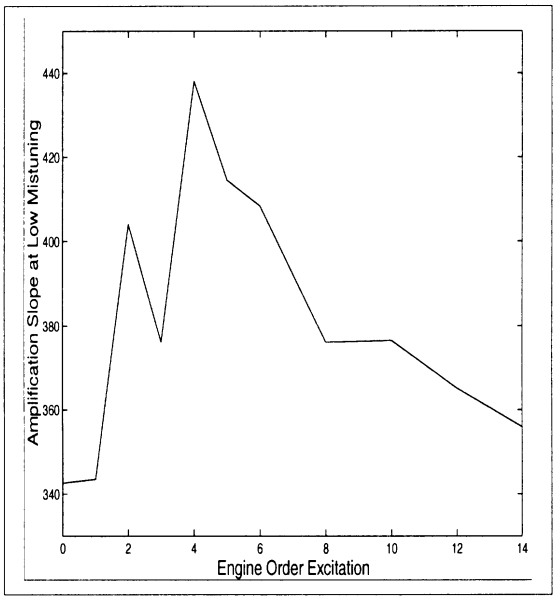

Figure 25. Variation of amplification-mistuning slope at low mistuning with engine order excitation for the 3W mode family.

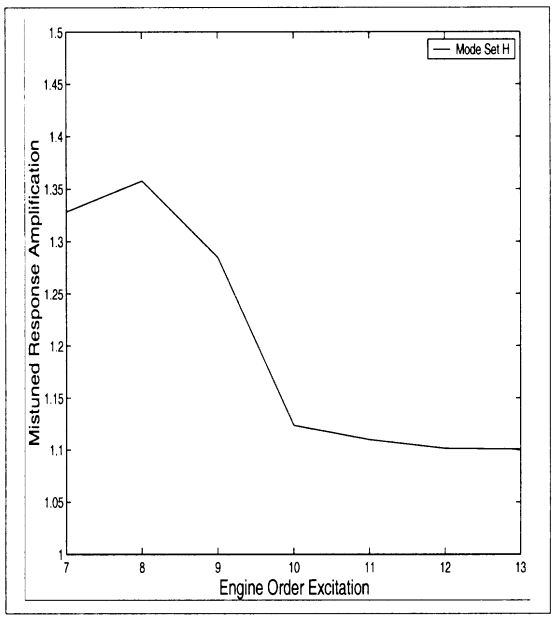

Figure 26. Variation of mistuning sensitivity with engine order excitation for the mixed 4W/1R mode set.

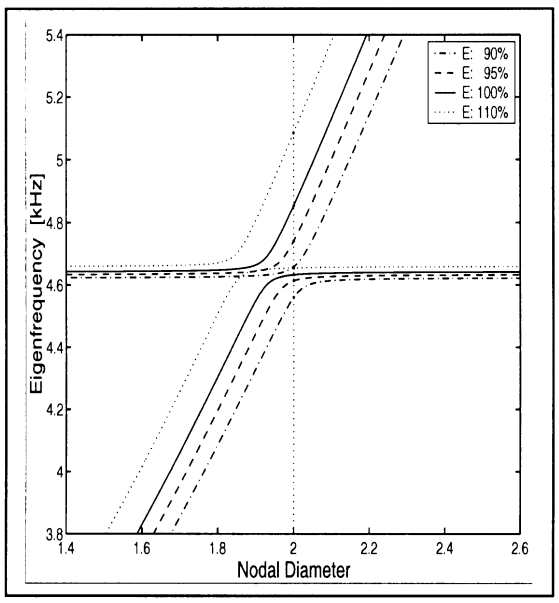

Figure 27. Eigenfrequency loci for different values of disk stiffness. Note the shifting of the 'center' of the curve veering.

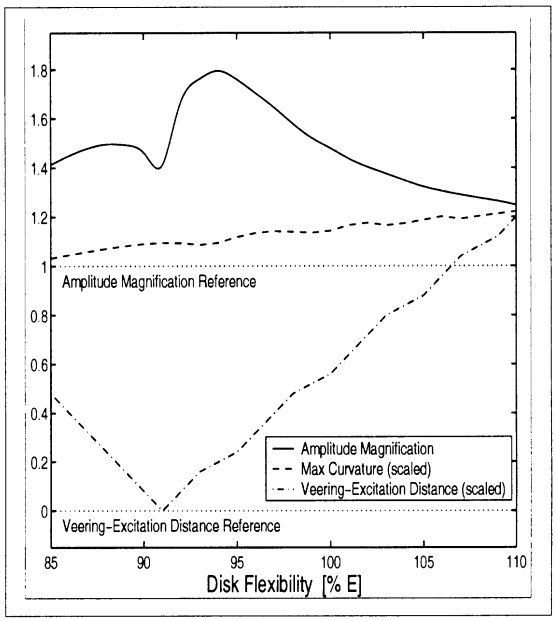

Figure 28. Relationship between mistuning sensitivity and nodal diameter distance from veering. This relationship is produced by varying disk flexibility, hence varying location of veering from the value of applied engine order excitation.

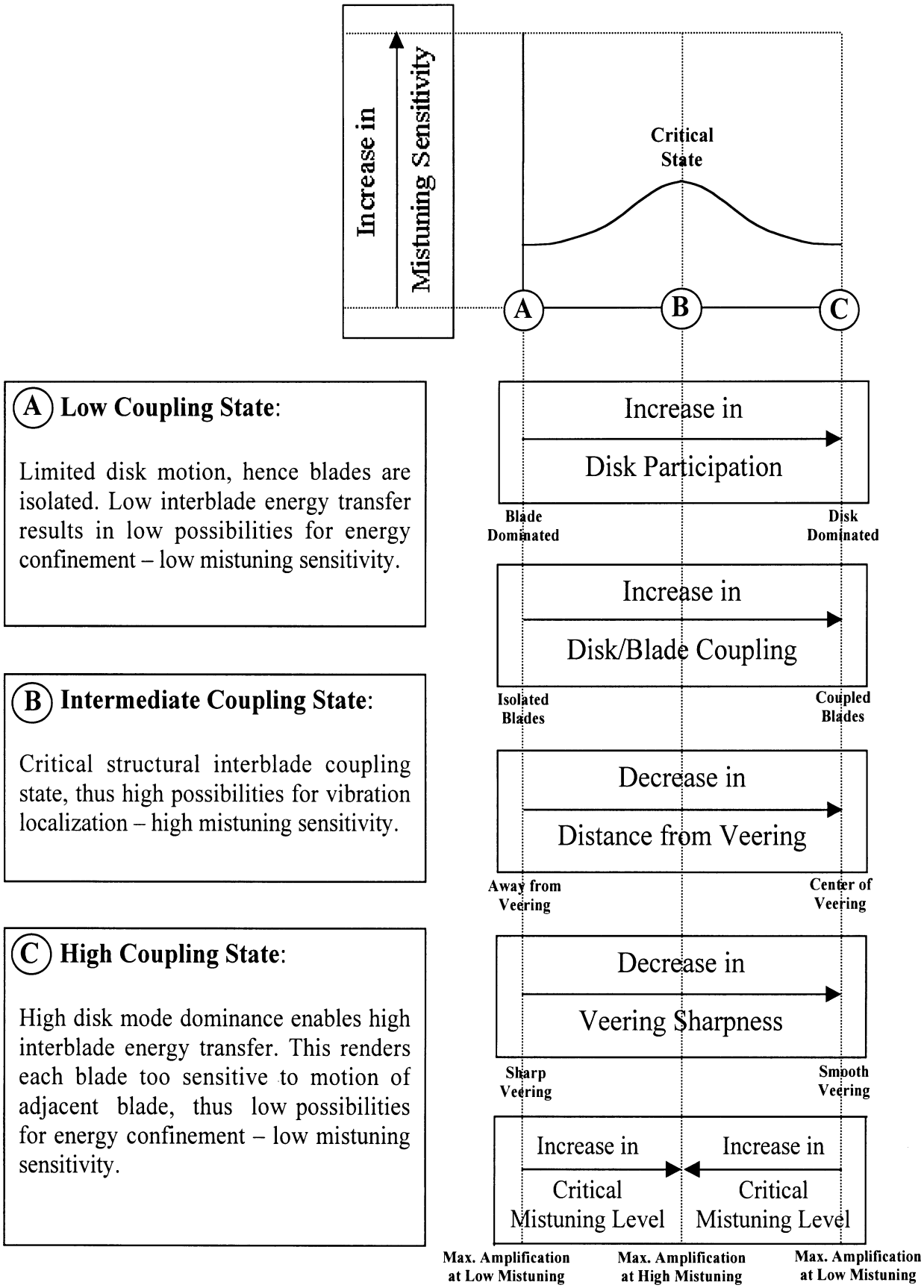

(A) Low Coupling State:

Limited disk motion, hence blades are isolated. Low interblade energy transfer results in low possibilities for energy confinement – low mistuning sensitivity.

(B) Intermediate Coupling State:

Critical structural interblade coupling state, thus high possibilities for vibration localization – high mistuning sensitivity.

(C) High Coupling State:

High disk mode dominance enables high interblade energy transfer. This renders each blade too sensitive to motion of adjacent blade, thus low possibilities for energy confinement – low mistuning sensitivity.

Figure 29. Schematic diagram describing, qualitatively, the relationship between mistuning sensitivity and the various system and operation variables. Also, a description of the physical mechanisms behind MS is outlined.

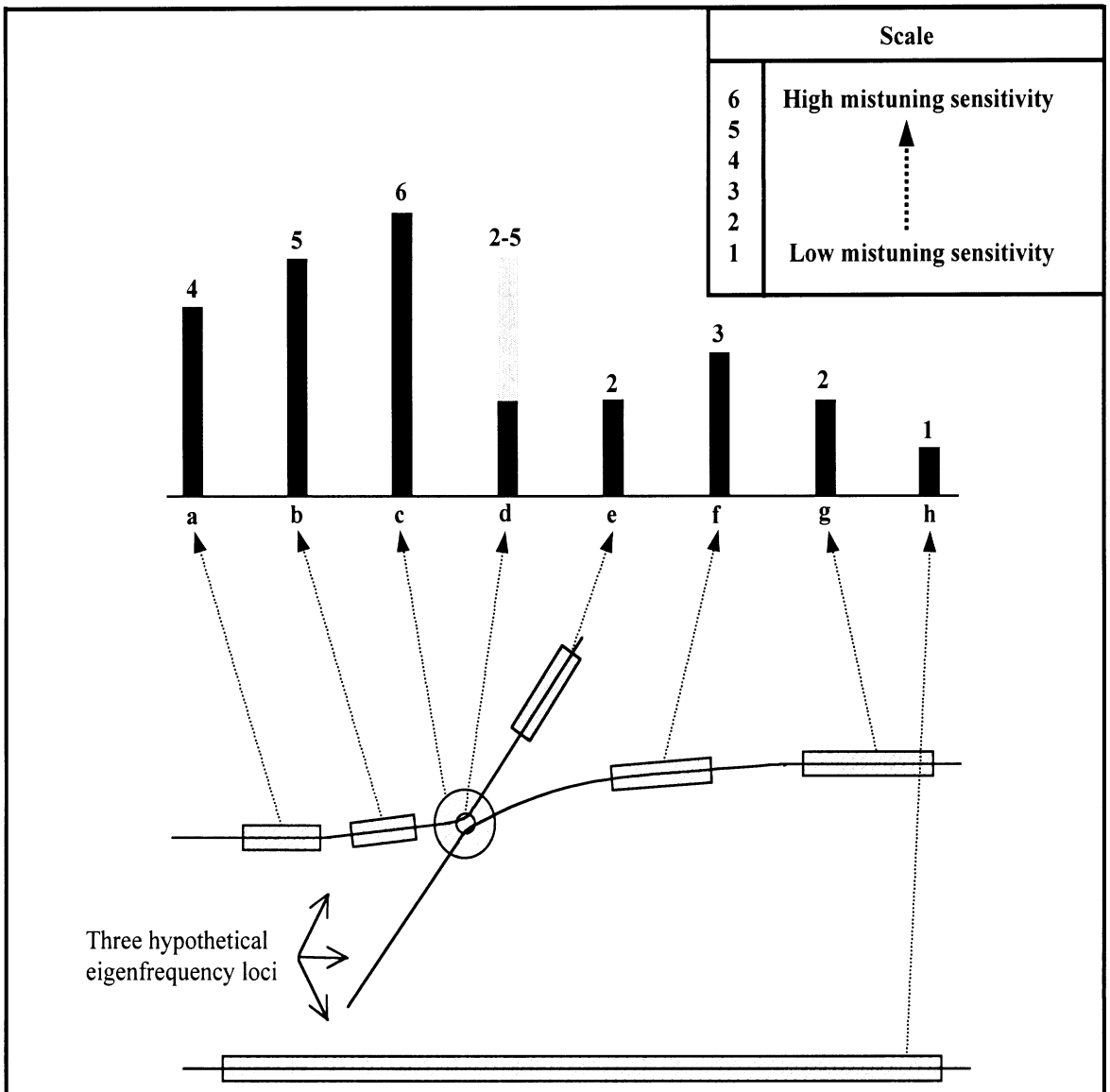

Zone	a	b	c	d
Description	Blade dominated, close to veering	Mixed mode, close to veering	Around 'center' of veering	At 'center' of veering
Source	Fig. 15-16; EOE: 3, 4	Fig. 17; EOE: 1	Fig. 14-17, 18-21; EOE closest to veering	Fig. 27-28; E ≈ 91%
Comments	MS increases as distance to veering decreases, *not recommended zone*	MS highest at critical loci slope; *dangerous zone*	MS depends on curve veering curvature; *dangerous zone*	Highly unstable, *dangerous zone*
Zone	**e**	**f**	**g**	**h**
Description	Disk dominated, away from veering	Mixed mode, away from veering	Blade dominated, away from veering	Blade dominated, no veering in loci
Source	Table 2	Fig. 26; EOE: 7-9	Fig. 26; EOE: 10-13	Reference [18]
Comments	*Safe zone*	MS highest at critical loci slope, *not recommended zone*	*Safe zone* (unless at critical Nodal Diameter)	*Safe zone* (unless at critical Nodal Diameter)

Figure 30. Schematic diagram classifying the various operation zones and the corresponding 'anticipated' mistuning sensitivity, with reference to source(s) of information, and comments on operational safety.